Circulation: Arrhythmia and Electrophysiology

ORIGINAL ARTICLE

Lesion Index Titration Using Contact-Force Technology Enables Safe and Effective Radiofrequency Lesion Creation at the Root of the Aorta and Pulmonary Artery

BACKGROUND: Ablation of some myocardial substrates requires catheter-based radiofrequency delivery at the root of a great artery. We studied the safety and efficacy parameters associated with catheter-based radiofrequency delivery at the root of the aorta and pulmonary artery.

METHODS: Thirty-six pigs underwent in-vivo catheter-based ablation under continuous contact-force and lesion index (power, contact-force, and time) monitoring during 60-s radiofrequency delivery with an open-irrigated tip catheter. Twenty-eight animals were allocated to groups receiving 40 W (n=9), 50 W (n=10), or 60 W (n=9) radiofrequency energy, and acute (n=22) and chronic (n=6) arterial wall damage was quantified by multiphoton microscopy in ex vivo samples. Adjacent myocardial lesions were quantified in parallel samples. The remaining 8 pigs were used to validate safety and efficacy parameters.

RESULTS: Acute collagen and elastin alterations were significantly associated with radiofrequency power, although chronic assessment revealed vascular wall recovery in lesions without steam pop. The main parameters associated with steam pops were median peak temperature >42°C and impedance falls >23 ohms. Unlike other parameters, lesion index values of 9.1 units (interquartile range, 8.7–9.8) were associated with the presence of adjacent myocardial lesions in both univariate (P=0.03) and multivariate analyses (P=0.049; odds ratio, 1.99; 95% CI, 1.02–3.98). In the validation group, lesion index values using 40 W over a range of contact-forces correlated with the size of radiofrequency lesions (R^2=0.57; P=0.03), with no angiographic or histopathologic signs of coronary artery damage.

CONCLUSIONS: Lesion index values obtained during 40 W radiofrequency applications reliably monitor safe and effective lesion creation at the root of the great arteries.

VISUAL OVERVIEW: A visual overview is available for this article.

José Manuel Alfonso-Almazán, MSc
Jorge G. Quintanilla, MScEng, PhD
María Jesús García-Torrent, PhD
Santiago Laguna-Castro, MSc
Cruz Rodríguez-Bobada, MVC, PhD
Pablo González, MVC
Juan José González-Ferrer, MD, PhD
Pablo Salinas, MD, PhD
Victoria Cañadas-Godoy, MD, PhD
Javier Moreno, MD, PhD
Luis Borrego-Bernabé, MD
Nicasio Pérez-Castellano, MD, PhD
José Jalife, MD
Julián Perez-Villacastín, MD, PhD
David Filgueiras-Rama, MD, PhD

Key Words: aorta ■ catheter ablation ■ contact force ■ elastin ■ pulmonary artery

https://www.ahajournals.org/journal/circep

WHAT IS KNOWN?

- Certain myocardial substrates require delivery of catheter-based radiofrequency energy at the root of the aorta or the pulmonary artery to target either a direct supravalvular myocardial sleeve or a contiguous myocardial territory.
- This procedure carries a risk of wall damage and potential fatal consequences, which have not been evaluated to identify ablation parameters associated with safe and effective radiofrequency delivery.

WHAT THIS STUDY ADDS?

- Catheter-based radiofrequency delivery at the root of the aorta or pulmonary artery under clinically relevant conditions in vivo generates acute arterial wall damage reflected in elastin and collagen fiber alterations, although chronic assessment revealed vascular wall recovery in lesions without steam pop.
- The ablation parameters associated with steam pop were high power (50 W, 60 W), peak impedance falls ≥23 ohms, and peak temperatures ≥42°C during radiofrequency delivery.
- Lesion index titration with different contact force ranges during 40 W radiofrequency applications correlated directly with the size of established myocardial lesions adjacent to the left coronary sinus and was not associated with angiographic or histological signs of coronary artery damage.

Catheter-based radiofrequency delivery is a well-established therapeutic approach to target and eliminate multiple types of arrhythmogenic substrates.[1–3] Most catheter-based procedures are performed from inside the heart and result in successful ablation of the target region.[2,3] However, certain myocardial substrates require delivery of radiofrequency energy at the root of the aorta or the pulmonary artery. For example, some ventricular arrhythmias arise from myocardial sleeves above the aortic or pulmonary valve, and radiofrequency delivery at these locations successfully eliminates the arrhythmia.[4,5] In other instances, although the arrhythmogenic substrate is not located above the semilunar valves, their unique anatomic location can allow the catheter to be brought into proximity with target atrial or ventricular regions, which can be successfully ablated from the aortic sinuses of Valsalva.[6–8]

Radiofrequency delivery at the endothelial side of a great artery can target either a direct supravalvular myocardial sleeve or a contiguous myocardial territory, but the procedure carries a risk of wall damage and potential fatal consequences.[9,10] However, there are scarce data available about acute or chronic damage to the arterial wall after radiofrequency delivery at the root of the aorta or pulmonary artery.[9] Moreover, optimal ablation and safety parameters have not been evaluated for in vivo radiofrequency delivery at these locations using current tip-irrigated catheters.[11] Monitoring of contact force (CF) and lesion index (LSI; incorporating power, contact-force, and time)[12–14] provides a suitable way to reliably define parameters that increase safety although creating effective ablation lesions in the myocardium adjacent to the arterial wall.

This knowledge gap in evidence-based radiofrequency ablation cannot readily be addressed with ex vivo human or animal experimental preparations; on the contrary, in vivo studies in humans would have limited capacity to extensively characterize arterial wall damage and lesion size. We have, therefore, used an in vivo pig model of catheter-based CF and LSI-monitored radiofrequency delivery to precisely characterize arterial wall damage and adjacent myocardial lesions in ex vivo samples after heart removal. The specific study goals were as follows: (1) to study lesion size and microscopic vascular damage after CF-guided radiofrequency delivery at the aorta or pulmonary artery; (2) to determine and validate the ablation parameters that create effective myocardial lesions adjacent to the arterial wall with minimal risk of arterial wall damage; and (3) to study vascular structural changes and potential functional consequences of chronic radiofrequency lesions created at the aortic root.

METHODS

The data that support the findings of this study are available from the corresponding author on reasonable request.

Study Design

The study population was divided into 2 experimental groups: Group I (n=28), used to assess safety and efficacy parameters at 3 power settings (40 W, 50 W, and 60 W), and group II (n=8), used to validate the ablation parameters associated with safe and effective lesion creation in group I (Figure 1). Group I animals were divided into 2 subgroups for the assessment of acute and chronic vascular damage after radiofrequency delivery. In total, 22 adult male Pietrain pigs (≈50 kg) were included in the acute subgroup and 6 similar pigs in the chronic subgroup. Group I animals were allocated to each subgroup according to radiofrequency power as follows: 40 W (n=7, acute; n=2, chronic), 50 W (n=8, acute; n=2, chronic), and 60 W (n=7, acute; n=2, chronic). In the acute subgroup, ablation lesions were created at 4 locations: the left aortic sinus, the noncoronary aortic sinus, and above and below the pulmonary valve in the root of the pulmonary artery. When lesions were incomplete (eg, because of catheter displacement during radiofrequency delivery) an additional lesion was created at the level of the right aortic sinus. In the chronic subgroup, only 1 lesion was created by radiofrequency delivery in the aortic root, at either the left aortic sinus or the noncoronary aortic sinus. In Group II, all ablations were performed by radiofrequency delivery at the left aortic sinus, and all animals underwent coronary angiography to assess potential acute injury to the left main coronary artery.

On completion of the ablation protocol, Group I animals in the acute subgroup were euthanized and the hearts removed.

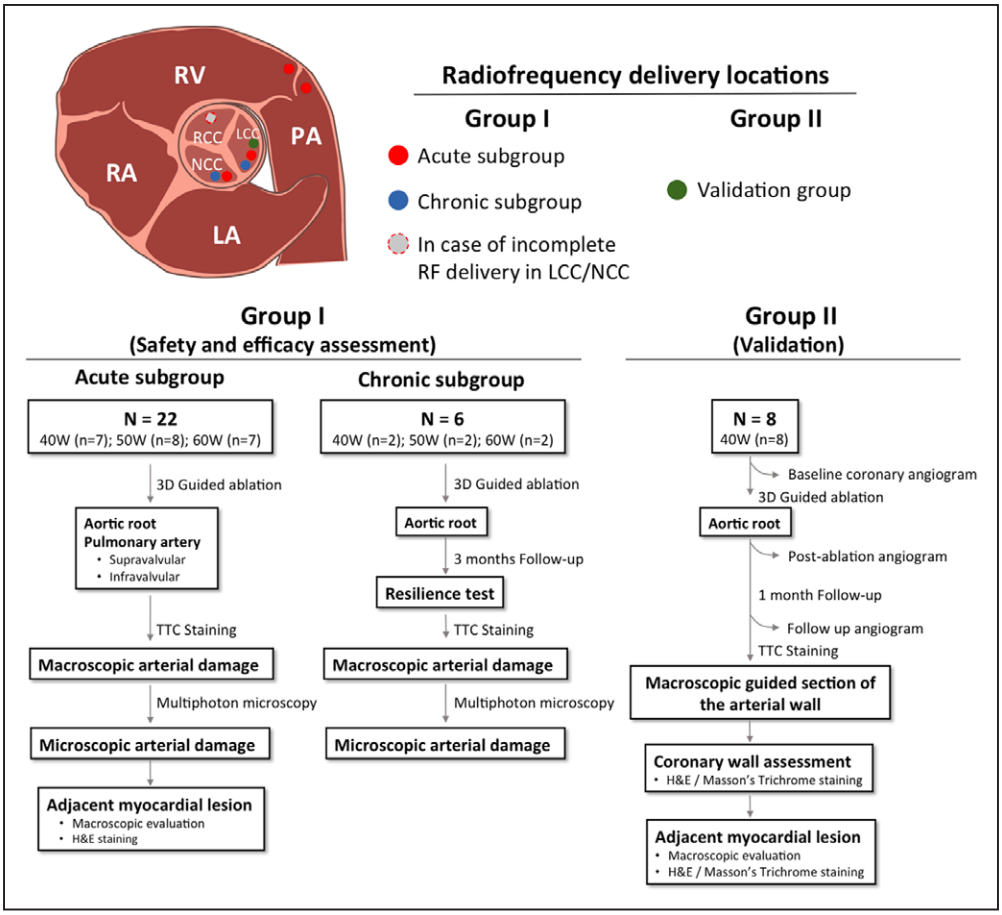

Figure 1. Experimental flow-chart.
LA indicates left atrium; LCC, left coronary cusp; NCC, noncoronary cusp; PA, pulmonary artery; RA, right atrium; RCC, right coronary cusp; RF, radiofrequency; RV, right ventricle; and TTC, triphenyltetrazolium chloride.

Group I animals in the chronic subgroup were followed up for 3 months after the ablation procedure to assess hemodynamic resilience and microscopic vascular healing at chronic stages. In group II, all pigs were followed up for 1 month after the ablation procedure to assess potential coronary damage at chronic stages and further quantify the radiofrequency lesions. A study flow-chart is shown in Figure 1.

The study was locally reviewed and approved in accordance with European guidelines (2010/63/EU) for the use and care of laboratory animals. Interventional procedures and heart excision were performed under general anesthesia. Animals were premedicated with ketamine (20 mg/kg, IM) and propofol (6 mg/kg IV), and general anesthesia was maintained with 2% isoflurane, atracurium besylate (1.25 mg/kg per hour IV), and fentanyl (0.005 mg/kg per hour IV).

Ablation Procedure

Pigs underwent catheter-based radiofrequency ablation using a 7-French, 3.5 mm open-tip irrigated catheter, which incorporates a force sensor in its distal portion (TactiCath Quartz, St Jude Medical, St Paul, MN). The catheter was introduced under fluoroscopy guidance into the vascular system from the right femoral vein to reach the right ventricular outflow tract or from the right femoral artery to reach the aortic root. The aorta and pulmonary artery were 3D reconstructed using an electroanatomic mapping system (Ensite Classic, St Jude Medical). Catheter positioning at each ablation target was ensured with electroanatomic guidance. The catheter tip was continuously irrigated with heparinized (1000 U/L) saline solution at 2 mL/min during navigation and at 30 mL/min during radiofrequency delivery, according to manufacturer instructions. Intravenous lidocaine was infused continuously (3 mg/kg per hour) throughout the procedure to decrease the risk of radiofrequency-related ventricular fibrillation.

The radiofrequency generator was programmed in power control mode, clearing the cutoff settings for temperature control, and adjusting the impedance settings to the lowest and highest limits. All ablation lesions were created by radiofrequency delivery for 60 seconds (CF, 10–40*g*) unless a steam pop, ventricular fibrillation, or catheter displacement occurred. If there was ventricular fibrillation, radiofrequency delivery was suspended, and a direct-current shock was delivered with an external defibrillator. Steam pops were identified by an audible pop associated with a decrease in impedance. Power, CF, temperature, impedance, LSI, and force-time integral were continuously monitored throughout each radiofrequency delivery using a TactiSys Quartz System (St Jude Medical).

Coronary Angiograms

All animals from group II underwent 3 sequential coronary angiograms, at baseline, after ablation, and at 1

month of follow-up; the vascular system was accessed via a femoral artery using a 5- or 6-French Amplatz left guiding catheter, and selective contrast injections were delivered into the ostium of the left main coronary artery. A set of 3 angiographic images (right anterior oblique 30°, right anterior oblique 30°+caudal 30°, and right anterior oblique 30°+cranial 30°) were obtained at each sequential time point by a trained interventional cardiologist. The minimum lumen diameter of the left main coronary artery was determined in each projection by image analysis with XA 7.3.48.0 (Medis Medical Imaging Systems, the Netherlands).

Macroscopic Assessment of Vascular and Myocardial Lesions

Pigs were euthanized with thiopental (10 mg/kg IV), and the heart was removed via median sternotomy. The heart was placed in 10% triphenyltetrazolium chloride at 40°C for 30 minutes.[15,16] Radiofrequency lesions are characterized by

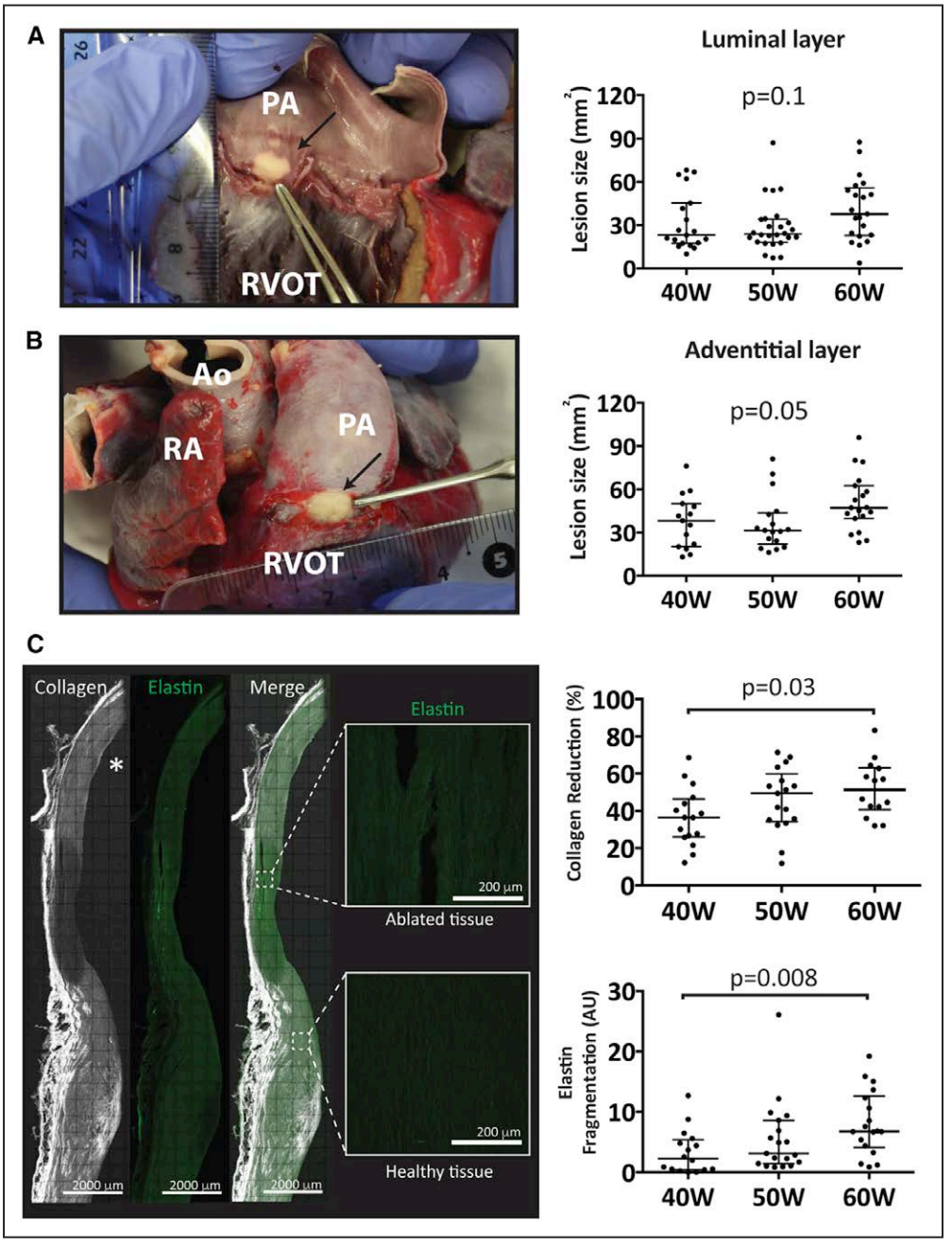

Figure 2. Macroscopy and multiphoton microscopy assessment of the arterial wall.
A and **B**, **Left** show macroscopic views of sample radiofrequency lesions on the luminal/endothelial (**A**) and adventitial (**B**) sides of the pulmonary artery (PA; black arrows). Graphs on the right show macroscopic lesion area on the luminal and adventitial sides of the aorta or PA and corresponding power settings. **C**, The **left** shows a sample multiphoton microscopy scanning of the aorta (cross-sectional view). Collagen and elastin images from the ablated region and surrounding tissue are depicted in gray-scale and green, respectively. The asterisk indicates the luminal side. The graphs on the right show the percentage of acute collagen signal reduction and quantification of elastin fragmentation in the ablated region relative to the surrounding tissue for each power setting. Ao indicates aorta; RA, right atrium; and RVOT, right ventricular outflow tract.

the absence of staining compared with nonablated areas (Figure 2A). The heart was then fixed in 4% formalin for at least 14 days. The pulmonary artery and aorta were both sectioned longitudinally to reveal lesions, and pictures were taken of the luminal and external arterial wall surfaces (Figure 2A and 2B). Images were analyzed with the ImageJ open source image-processing tool (National Institutes of Health) to measure lesion area.[17] The arteries were then cross-sectioned at the maximum diameter of the radiofrequency lesion for further microscopy analysis.

Myocardial lesions adjacent to the target area were measured using ImageJ software. The absence of an overt radiofrequency lesion in the adjacent myocardium after triphenyltetrazolium chloride staining was registered as a radiofrequency application with no associated overt macroscopic myocardial damage.

Microscopic Vascular Scanning

In group I, the microscopic structure of the arterial wall was assessed by multiphoton microscopy. The arteries were immersed in 70% formalin/30% sucrose solution overnight at 4ºC and embedded in optimal cutting temperature compound. The tissue samples were cut into 30 µm thick cross-sections, which were examined directly by overnight multiphoton microscopy scanning at ×20. Both the lesion region of interest and the surrounding healthy area of the artery were scanned. Samples were excited at 800 nm, and second harmonic generation signals originating from collagen were obtained at 400 nm (Figure 2C). Elastin autofluorescence signals were obtained at 450 to 650 nm. Collagen reduction because of radiofrequency delivery was calculated as the collagen signal intensity in the region of interest relative to that in the surrounding nonablated tissue. Elastin fiber fragmentation was computed as the black void area among elastin fibers within the region of interest compared with the surrounding nonablated tissue.

Histopathology Analysis

In the group I acute subgroup, myocardial samples with overt macroscopic lesions were cross-sectioned at the maximum diameter to determine the depth and extent of acute necrosis. Myocardial cross-sections were dehydrated, embedded in paraffin, and cut into 10 µm thick sections. Hematoxylin and eosin (H&E) stained sections were digitized using a NanoZoomer S360 Digital slide scanner (Hamamatsu, Japan) for subsequent analysis. The necrotic area was delineated manually using ImageJ software, based on conventional histopathologic features of necrosis, including elongated and pyknotic nuclei, loss of the striated cardiomyocyte structure, slight increases in color intensity, and glassy cytoplasm.[18]

Table 1. Ablation Lesions and Ablation Parameters Within Each Experimental Group

	Group I						Group II
	Acute Subgroup			Chronic Subgroup			Validation
	40 W	50 W	60 W	40 W	50 W	60 W	40 W
Animals (n)	7	8	7	2	2	2	8
Weight (kg)	47.4 (46.0–50.7)	57.0 (53.5–61.4)	47.0 (43.3–48.4)	34.2–37.0	32.0–32.7	33.7–35.3	49.7 (47.9–52.4)
Ablation lesions (n)	29	32	30	2	2	2	8
Pulmonary artery							
Infravalvular	5	6	5	0	0	0	0
Supravalvular	10	6	11	0	0	0	0
Aortic root							
Noncoronary sinus	7	8	6	1	1	1	0
Left aortic sinus	7	8	6	1	1	1	8
Right aortic sinus	0	4	2	0	0	0	0
Ablation parameters							
Mean temperature (°C)	36.0 (33.0–37.0)	36.5 (36.0–38.8)	34.5 (32.3–36.0)	42.0–46.0	33.0–36.5	30.0–31.0	33.0 (33.0–33.5)
Max. temperature (°C)	38.0 (35.0–40.0)	38.0 (37.0–42.5)	38.5 (36.0–42.0)	44.0–49.0	35.0–38.0	33.0–34.0	35.0 (34.5–37.5)
Duration (w/o steam pop) (s)	60	60	60	60	60	60	60
Duration (with steam pop) (s)	36.0 (23.0–52.0)	46.5 (22.3–60.0)	29.0 (17.0–43.0)	N/A	N/A	N/A	N/A
Impedance drop (W)	16.0 (12.0–20.0)	12.5 (10.3–19.8)	21.5 (16.8–26.3)	4.0–8.0	12.0–15.0	10.0–17.0	15.0 (11.5–16.5)
Contact force (*g*)	17.0 (13.0–26.0)	17.0 (14.0–27.5)	12.5 (8.0–18.0)	20.0–25.0	16.0–21.0	16.0–18.0	22.5 (17.7–34.5)
FTI (*g**s)	922.0 (644.0–1572.0)	943.0 (711.0–1468.0)	648.0 (345.0–866.0)	1529.0–1171.0	966–1236	961.0–1099.0	1343.5 (1044.7–2093)
LSI (Units)	8.4 (7.1–9.0)	9.0 (8.3–10.3)	8.5 (6.6–8.9)	9.7–10	9.0–9.7	9.9–10.1	10.1 (9.5–11.2)
Steam Pop (n)	3	9	11	0	0	0	0

Data are represented as median (interquartile range). FTI indicates force-time integral; and LSI, lesion index.

In group II, additional Masson trichrome staining was used to assess established myocardial lesions and the vascular wall of the left main coronary artery.

Aortic Resilience Evaluation in Chronic Lesions

After a mean follow-up of 84 days (range, 70–96 days) from radiofrequency lesion creation, all animals from the group I chronic subgroup underwent cannulation of the left and right femoral arteries to progress a pigtail catheter to the ascending aorta (proximal, next to the aortic valve), and a second pigtail catheter to the thoracic descending aorta (distal) under fluoroscopy guidance. Open-chest surgery was then performed to expose the ascending aorta and the anterior part of the heart. The ascending aorta and main pulmonary artery were carefully separated to introduce a surgical clamp that embraced the aorta above both the chronic lesion and the proximal pigtail catheter. Left ventricular afterload was progressively increased on partial closure of the aortic clamp to test acute aortic resilience in the presence of a chronic radiofrequency lesion. Proximal and distal aortic pressures were continuously monitored and recorded at 100 samples/s (anesthetic equipment, Carecape Monitor, Datex-Ohmeda, General Electric Medical, Milwaukee). The acquired signals were imported into Matlab for further analysis using customized software.

Statistical Analyses

Continuous variables are reported as median and interquartile range [Q1–Q3] according to data distribution. Data normality was assessed with the Saphiro-Wilk test. The Student *t* test or the Mann-Whitney *U* test was used for 2-group comparisons, as appropriate. ANOVA or the Kruskal-Wallis test was used for

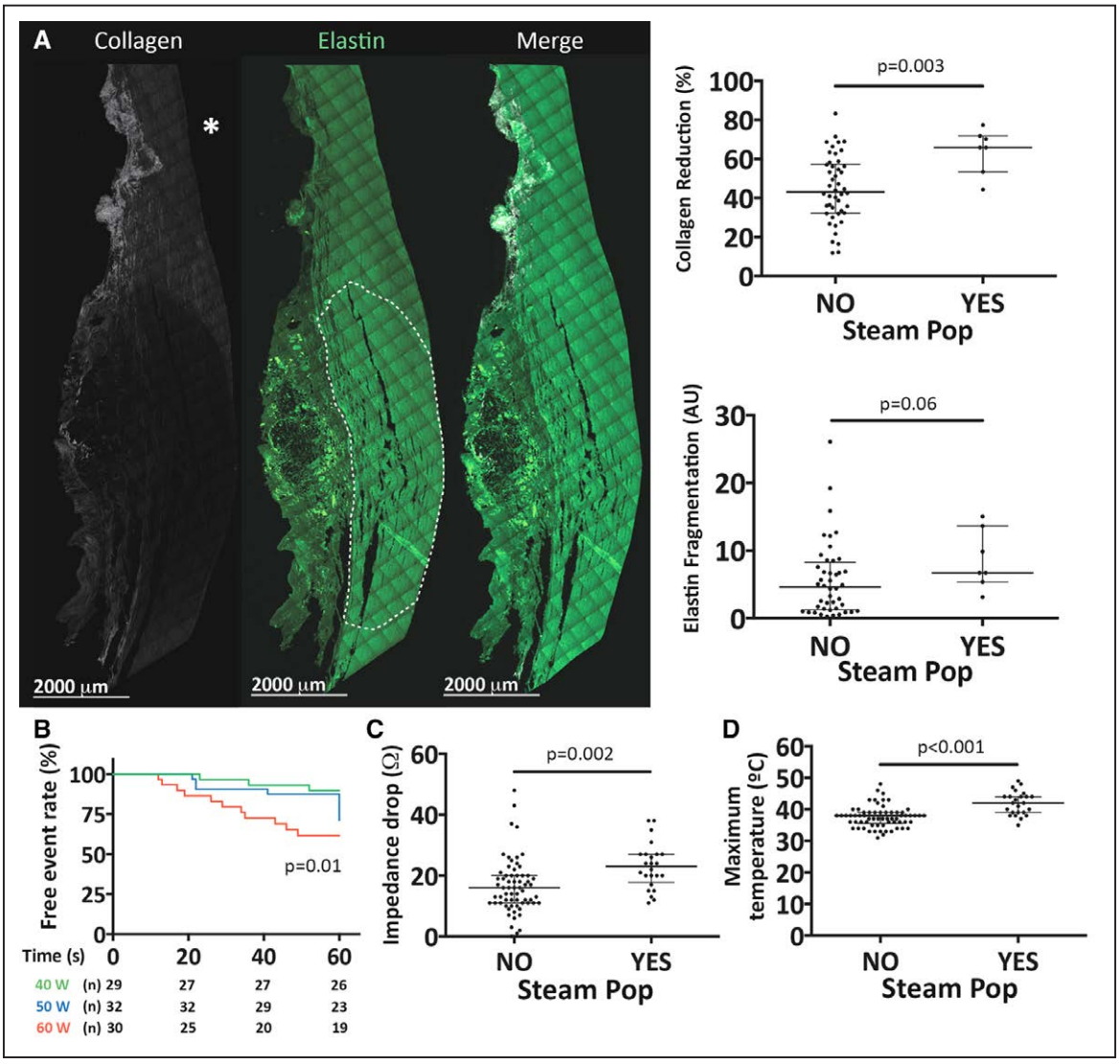

Figure 3. Structural vascular damage after steam pop and ablation parameters associated with steam pop.
A, Sample multiphoton microscopy scanning of the pulmonary artery (cross-sectional view). Collagen (gray-scale) and elastin (green) data from the ablated region show extensive collagen reduction and elastin fragmentation (area encircled by the dashed line). The asterisk indicates the luminal side. The graphs on the right show quantification of collagen signal reduction and elastin fragmentation for lesions with and without steam pop. **B**, Kaplan-Meier curves depicting steam pop events for each power-setting group. The log-rank test shows a statistically significant association with steam pop incidence in the 60 W group relative to the 40 W and 50 W groups. **C** and **D**, Impedance drop (**C**) and maximum peak temperature (**D**) in ablation lesions with and without vascular steam pop.

3-group comparisons according to data distribution. Kaplan-Meier plots were used to depict the elapsed time-to-steam pop, together with global and paired comparisons (log-rank test). The multivariate analysis included physiological relevant variables (ie, animal weight) and statistically significant variables associated with steam pop or the presence of adjacent myocardial lesions in the univariate analysis. A binary logistic regression was used to identify the main parameters associated with the presence of adjacent myocardial lesions. A Cox regression analysis was performed to identify the ablation parameters associated with time-to-steam pop. Differences were considered statistically significant at $P<0.05$. All data were analyzed with GraphPad Prims6 (GraphPad Software Inc, California) except for the multivariate analysis, which was run with SPSS 20.0 (IBM Corp, New York).

RESULTS

Descriptive data on ablation lesions and ablation parameters within each experimental group are shown in Table 1.

High Radiofrequency Power Increases Acute Macroscopic and Microscopic Arterial Wall Damage

Macroscopic assessment of the arterial wall showed a statistical trend to larger lesion areas on the endothelial/luminal layer with increasing radiofrequency power (40 W, 23.1 mm^2 [17.5–45.3 mm^2]; 50 W, 23.8 mm^2 [18.2–34.0 mm^2]; and 60 W, 37.7 mm^2 [22.7–55.8 mm^2]; P=0.1; Figure 2A). For the adventitial layer, this difference was statistically significant, with 60 W radiofrequency generating larger lesions than 50 W or 40 W applications (47.1 mm^2 [39.8–62.6 mm^2] versus 31.4 mm^2 [22.0–43.7 mm^2] and 38.2 mm^2 [20.2–50 mm^2], respectively; P=0.05; Figure 2B).

Radiofrequency-associated acute vascular damage was reflected in reduced vascular collagen detected as a decrease in second harmonic generation signals on multiphoton microscopy images (Figure 2C). Radiofrequency lesions also affected vascular elastin fibers, which showed several degrees of rupture with evident fragmentation and loss of continuity, losing their typical sinusoidal curvature (Figure 2C). Excluding radiofrequency lesions with steam pop, collagen reduction was significantly higher in the 60 W group than in the 40 W group (51.3% [40.7%–63.2%] versus 36.5% [26.0%–46.4%]; P=0.03; Figure 2C). Elastin fiber disruption was also significantly more pronounced at 60 W than at 40 W (6.8 AU [4.1–12.6 AU] versus 2.5 AU [0.5–5.5 AU]; P=0.008; Figure 2C).

LSI and Force-Time Integral Values Show No Association With Steam Pop Incidence

Steam pops occurred in 23 out of 91 radiofrequency lesions in the acute subgroup, although macroscopic assessment showed different degrees of arterial wall disruption among animals (Figure 1 in the Data Supplement). Microscopy analysis of steam pop consequences in the arterial wall showed a significantly larger reduction in vascular collagen than in lesions without steam pop (65.8% [53.5%–71.8%] versus 43.2% [32.3%–57.3%]; P=0.003; Figure 3A). Lesions with steam pop also showed a trend toward more extensive elastin fragmentation (6.7 AU [5.3–13.6 AU] versus 4.6 AU [1.2–8.2 AU]; P=0.06; Figure 3A).

The incidence of steam pops increased with power, rising from 10.0% at 40 W to 28.1% at 50 W, and 36.6% at 60 W (P=0.02). The median elapsed time-to-steam pop was shorter at 60 W than at 50 W and 40 W (29.0 [17.0–43.0]; 46.5 [22.3–60.0]; and 36.0 [23.0–52.0], respectively; P=0.01; Figure 3B). Cox regression analysis showed a statistically significant association between radiofrequency power and time-to-steam pop (P=0.037; hazard ratio, 1.06; 95% CI,

Table 2. Ablation Parameters Associated With Steam Pop Incidence in Univariate Analysis

Univariate Analysis	Steam Pop		
Variable	No	Yes	*P* Value
Power			0.02
40 W	26	3	
50 W	23	9	
60 W	19	11	
Contact force (*g*)	15.0 (12.0–21.0)	16.0 (10.0–27.0)	0.4
FTI (*g*·s)	910.0 (712.3–1267.0)	573.0 (306.0–1145.0)	0.01
LSI (U)	8.8 (8.1–9.7)	7.9 (6.7–8.9)	0.06
Max. temperature (°C)	38.0 (35.0–39.0)	42.0 (39.0–44.00	<0.001
Impedance drop (Ω)	16.0 (11.0–20.0)	23.0 (17.75–27.0)	0.002
Animal weight (kg)	51.0 (45.0–55.2)	47.0 (45.2–53)	0.7

FTI indicates force-time integral; LSI, lesion index; and Max, maximum.

Table 3. Ablation Parameters Associated With Time-to-Steam Pop in Cox Regression Analysis

Cox Regression Analysis	Time-to-Steam Pop			
Variable	*P* Value	Hazard Ratio (HR)	95% CI HR	
Power	0.037	1.06	1.003	1.120
Max. temperature	<0.001	1.24	1.124	1.366
Impedance drop	0.009	1.07	1.016	1.122

Max indicates maximum.

1.003–1.120). Neither LSI nor force-time integral values were statistically associated with steam pops (Tables 2 and 3). Importantly, shorter radiofrequency time in lesions with steam pop yielded lower values of both LSI and force-time integral compared with lesions without steam pop (Tables 1 and 2). However, univariate and Cox regression analyses both showed significant associations of time-to-steam pop with impedance fall (*P*=0.009; hazard ratio, 1.07; 95% CI, 1.016–1.122) and maximum temperature (*P*<0.001; hazard ratio, 1.24; 95% CI, 1.124–1.366; Figure 3C and 3D and Tables 2 and 3).

Aortic Wall Resilience is Unaffected in Chronic Lesions

All pigs allocated to the chronic subgroup survived the follow-up period with no vascular complications. Acute increases in left ventricular afterload and ascending aorta pressures (average mean aortic systolic/diastolic pressure: 228.7±17.1/109.5±12.7 mm Hg Figure 2 in the Data Supplement) over a mean period of 13.4±3.3 minutes were not associated with vascular complications in any of the 3 power setting groups. Microscopy assessment of chronic lesions showed overt signs

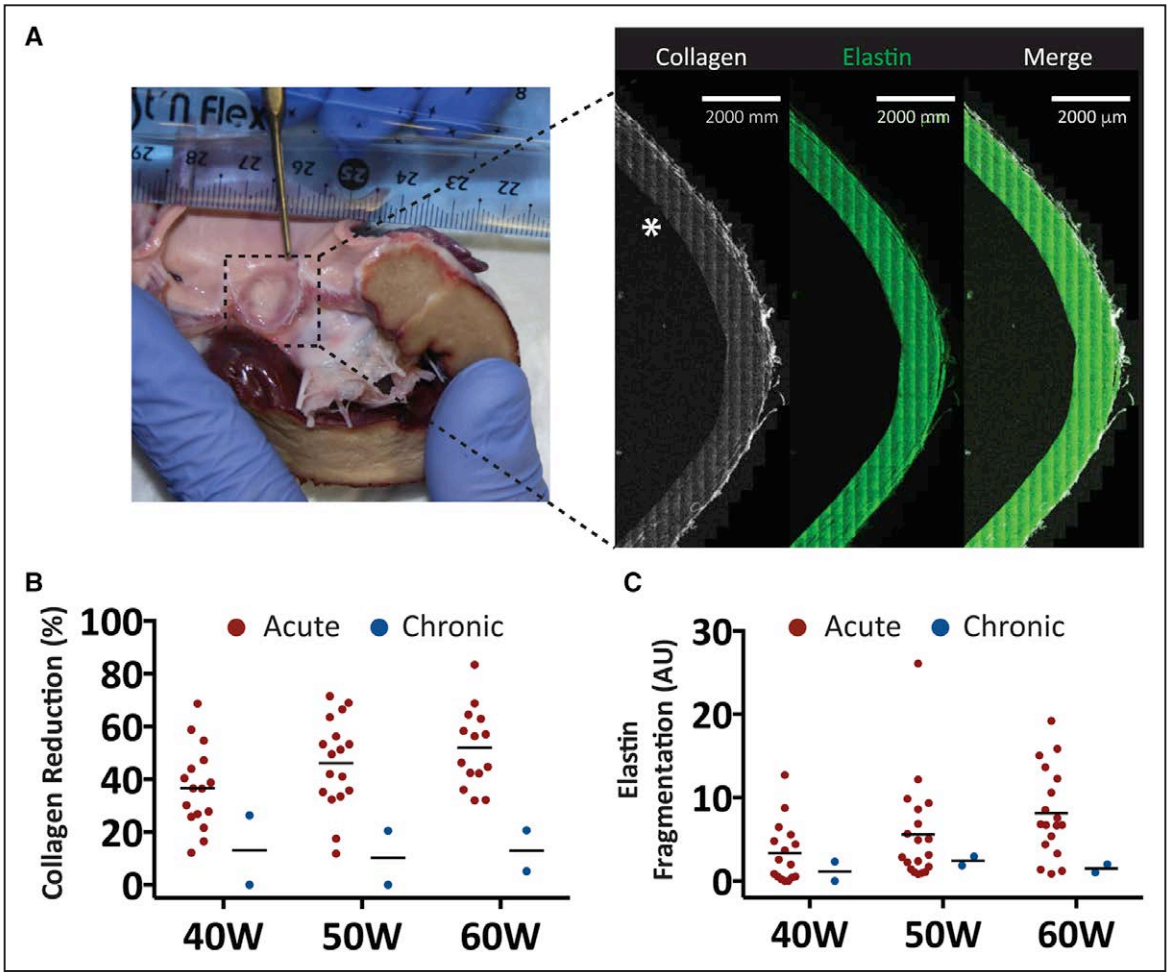

Figure 4. Chronic vascular damage after radiofrequency delivery.
A, Sample case of a chronic ablation lesion in the noncoronary aortic sinus. The **left** shows TTC staining in the excised heart. The **right** multiphoton microscopy scanning; the asterisk indicates the luminal side. **B** and **C**, Collagen signal reduction (**B**) and elastin fragmentation (**C**) in the ablated vascular wall after radiofrequency delivery (red-filled circles) and after ≈3 mo of follow up (blue-filled circles) for each power setting. Chronic lesions with no evident borders between the ablated area and surrounding tissue were analyzed as a whole sample.

of both collagen and elastin recovery compared with acute lesions (Figure 4). Importantly, none of the chronic radiofrequency lesions were associated with steam pop during acute radiofrequency delivery.

CF and LSI Values Predict the Presence of Adjacent Myocardial Lesions

The presence of acute adjacent myocardial lesions after radiofrequency delivery was significantly associated with higher values for CF (17.0*g* [14.0–22.0*g*] versus 12.5*g* [9.0–20.5*g*]; *P*=0.02; Figure 5A) and LSI (9.1 U [8.7–9.8 U] versus 8.1 U [7.0–9.1 U]; *P*=0.03; Figure 5A, Table 4). In the multivariate analysis, only LSI maintained a significant association with the presence of adjacent myocardial lesions (*P*=0.049; Table 5). Thus, the higher the LSI, the greater was the likelihood of successful ablation of adjacent myocardial tissue. Further histopathologic analysis showed a direct statistical trend for an association between LSI and larger necrotic area in the adjacent myocardial tissue (*P*=0.1; Figure 5B and 5C). In contrast, CF did not significantly correlate with the necrotic area in adjacent myocardial tissue (Figure 5D). Necrotic area showed no significant association with power setting (40 W, 4.6 mm^2 [2.5–13.7 mm^2]; 50 W, 6.2 mm^2

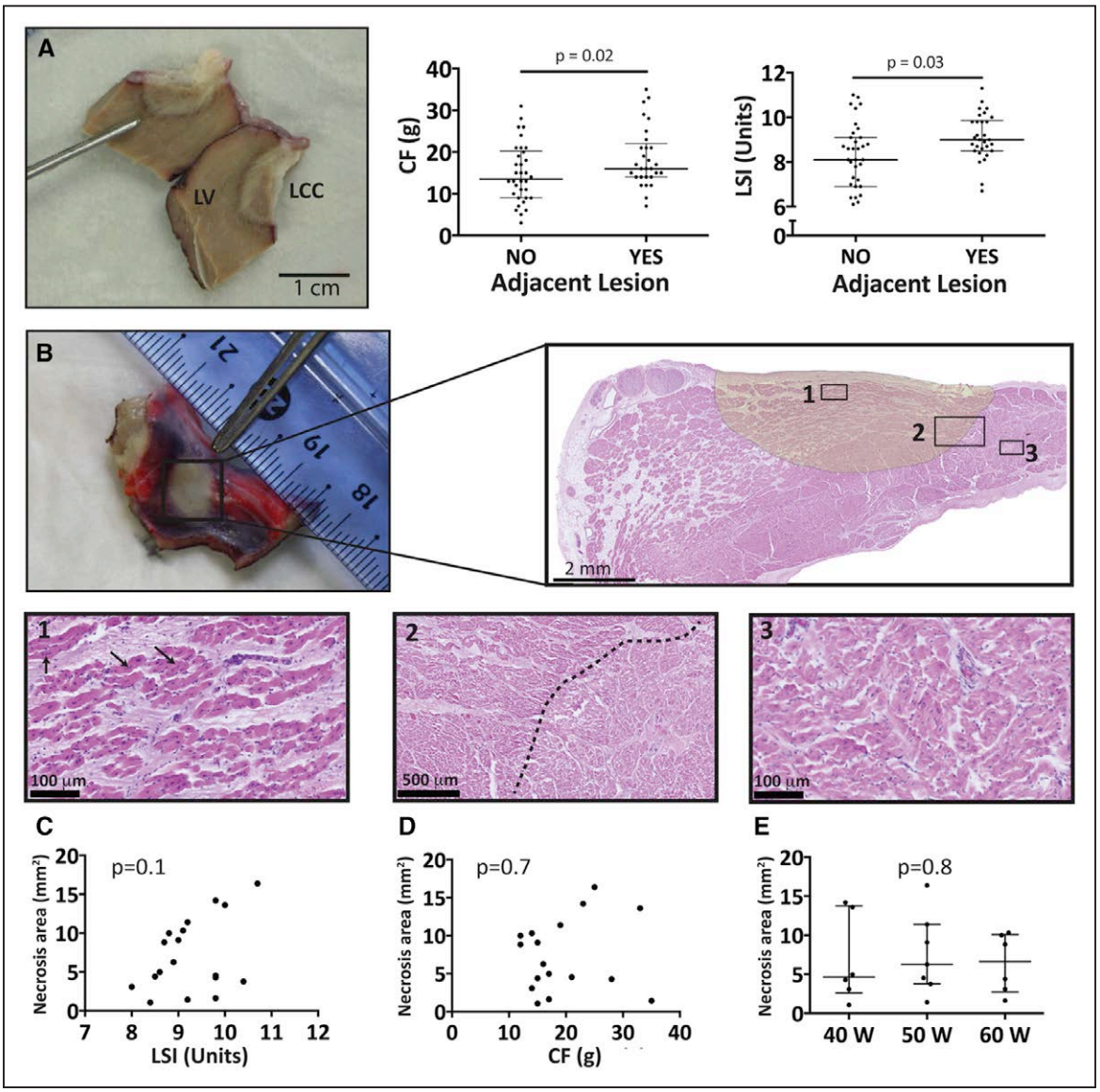

Figure 5. Acute macroscopic and microscopic lesion assessment in the myocardium adjacent to the arterial wall.
A, Sample myocardial lesion adjacent to the left coronary cusp (LCC). The graphs on the right show contact force and lesion index (LSI) values obtained in radiofrequency (RF) applications with and without acute adjacent myocardial lesions. **B,** The **left** shows a sample macroscopic view of an atrial myocardial lesion associated with RF delivery at the noncoronary aortic sinus. The **right** shows sample hematoxylin and eosin staining of the boxed region in the **left**. The numbered boxed areas are shown in high-power view below: necrotic area (1), the border zone between necrotic and healthy regions (2), and a healthy/nonablated area (3). Black arrows in 1 indicate typical elongated and pyknotic nuclei in necrotic areas. **C**, Relationship between necrotic area in the atrial myocardium adjacent to the noncoronary aortic sinus and LSI. **D**, Relationship between necrotic area in the atrial myocardium adjacent to the noncoronary aortic sinus and contact force (CF). **E**, Necrotic areas for each power-setting group.

Table 4. Ablation Parameters Associated With Acute Adjacent Myocardial Lesions in Univariate Analysis

Univariate Analysis	Adjacent Lesion		
Variable	No	Yes	*P* Value
Power (W)			0.9
40 W	11	10	
50 W	12	10	
60 W	9	9	
Contact Force (*g*)	12.5 (9.0–20.5)	17.0 (14.0–22.0)	0.02
FTI (*g*·s)	770.0 (520.3–1058.0)	964.5 (841.0–1300)	0.01
LSI (U)	8.1 (7.0–9.1)	9.1 (8.7–9.8)	0.03
Impedance drop (Ω)	13.5 (9.3–21.5)	15.5 (12.0–19.5)	0.52
Max. temperature (°C)	37.0 (34.3–39.0)	38.0 (36.0–39.0)	0.38
Animal weight (Kg)	49.7 (45.0–54.8)	52.2 (47.0–55.2)	0.8

FTI indicates force-time integral; LSI, lesion index; and Max, maximum.

[3.7–11.4 mm^2]; and 60 W, 6.6 mm^2 [2.7–10.1 mm^2]; *P*=0.8; Figure 5E).

LSI Correlates With Established Myocardial Lesions After Follow-Up

In group II, 4 pigs received a 40 W radiofrequency energy and ≈18 g of CF, parameters that produced effective and safe radiofrequency lesions in group I. In a further 4 pigs, the LSI was titrated by increasing the CF. Histopathologic analysis at 1-month follow-up showed that LSI significantly correlated with adjacent myocardial lesion area (R^2=0.58; *P*=0.03; Figure 6A through 6C) and lesion depth (R^2=0.67; *P*=0.01; Figure 6A through 6D). In contrast, CF did not correlate with adjacent myocardial lesion size (Figure 6E). Moreover, plotting LSI values at 10-s intervals revealed that CF modulation could be used to titrate LSI values over a 60-s radiofrequency delivery (Figure 6F).

Sequential coronary angiograms in group II animals revealed no signs of coronary stenosis (Figure 7A and 7B and Movie 1 in the Data Supplement). No significant differences were observed in the minimum lumen diameter of the left main coronary artery at baseline, immediately after ablation, and at 1-month follow-up (8.1 mm [7.0–8.8 mm], 7.9 mm [6.7–8.5 mm], and 7.7 mm [6.8–8.5 mm], respectively; *P*=0.7; Figure 7C). Further histological analysis of the left main coronary ostium confirmed the absence of signs of coronary injury (Figure 7D).

DISCUSSION

The main findings of this study show that catheter-based radiofrequency delivery at the root of the aorta or pulmonary artery under clinically relevant conditions in vivo generates acute arterial wall damage reflected in elastin and collagen fiber alterations at the microscopic level. This acute injury was directly related to radiofrequency power, although chronic assessment revealed vascular wall recovery in lesions without steam pop. The main parameters associated with steam pop were high power (50 W, 60 W), median impedance falls ≥23 ohms, and a median peak temperature ≥42°C during radiofrequency delivery. Unlike other ablation parameters, LSI was significantly associated with the presence of acute adjacent myocardial lesions. Moreover, LSI titration with different CF ranges during 40 W radiofrequency applications correlated directly with the size of established myocardial lesions adjacent to the left coronary sinus and was not associated with angiographic or histological signs of coronary artery damage.

Several studies have attempted to evaluate the relationship between ablation parameters and lesion size in the target myocardium.[13,15,19–21] In vitro preparations exclude analysis of important physiological conditions only present in vivo, such as blood flow or continuous catheter and heart motion in the beating heart. Recent data from Leshem et al[19] show that in vitro preparations often result in overestimation of lesion size, especially at high energy settings. In

Table 5. Ablation Parameters Associated With Acute Adjacent Myocardial Lesions in Multivariate Analysis

Multivariate Analysis	Adjacent Lesion			
Variable	*P* Value	Odds Ratio	95% CI Odds Ratio	
Contact force	0.3	0.87	0.63	1.12
FTI	0.4	1.01	0.99	1.01
LSI	0.049	1.99	1.02	3.98

FTI indicates force-time integral; and LSI, lesion index.

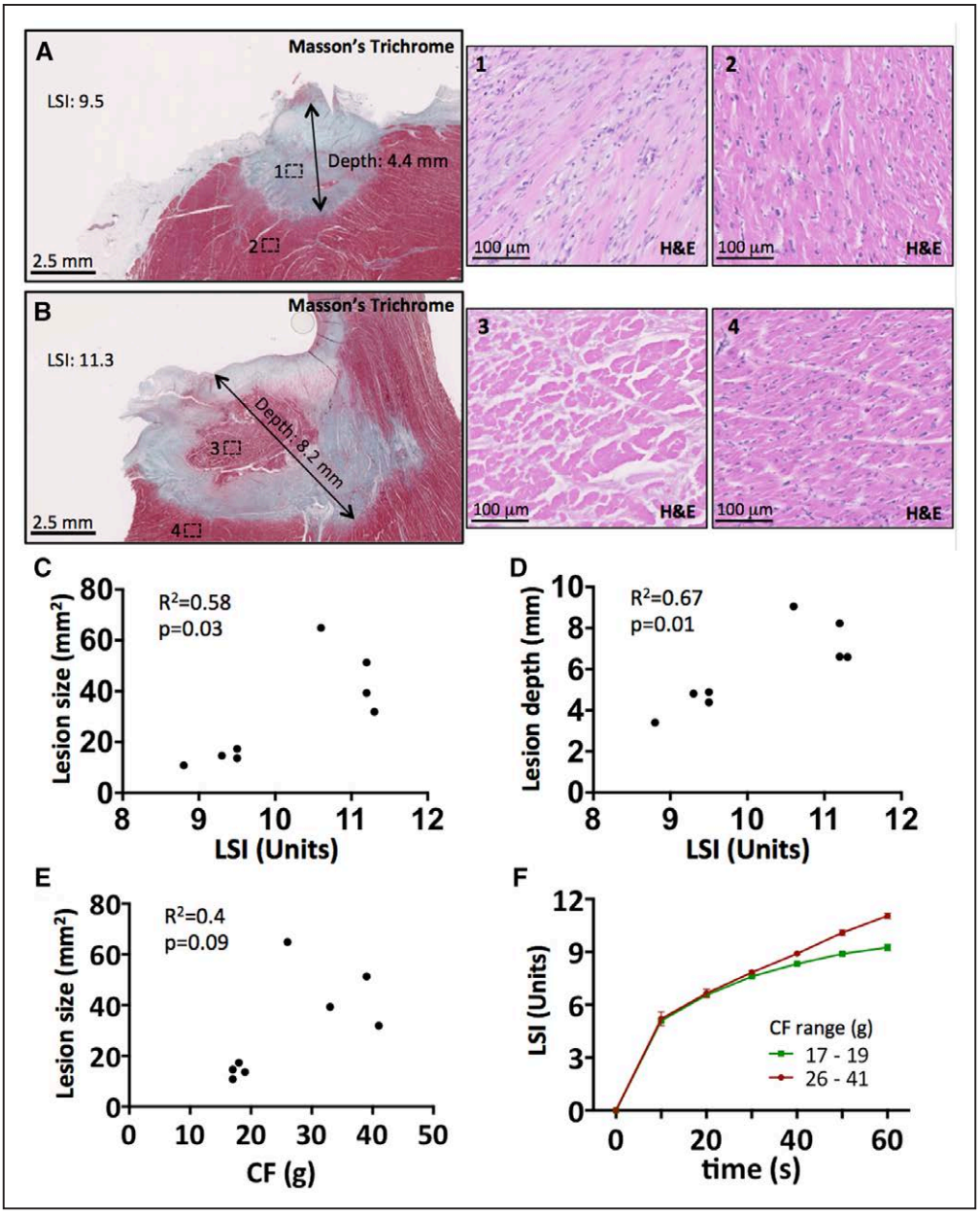

Figure 6. Lesion assessment in myocardial tissue adjacent to the arterial wall at 1-month follow-up.
A and **B**, Sample Masson trichrome-stained radiofrequency (RF) lesions in the myocardium adjacent to the left coronary sinus. The **right** show hematoxylin and eosin (H&E) staining of the numbered boxed areas at high-magnification. In 3, there is still no fibrosis 1 mo after RF delivery; however, there are also no viable cardiomyocytes. **C** and **D**, Relationship of LSI with adjacent myocardial lesion area (**C**) and lesion depth (**D**). **E**, Relationship between lesion area and contact force (CF). **F**, Mean±standard error LSI values at 10-s intervals for different CF ranges. LSI, lesion index.

addition to these intrinsic limitations, in vitro preparations cannot model the targeting of myocardial tissue across an intermediate vascular wall that may be damaged during the creation of the adjacent myocardial lesion. This drawback further highlights the importance of a clinically relevant in vivo experimental design as used here.

Our data show that macroscopic lesions on the arterial wall surface increased with radiofrequency power, with significantly more adventitial layer injury at 60 W than at 40 W and 50 W. This finding is consistent with a degree of endothelial and intimal layer preservation because of the use of an irrigated-tip catheter, in combination with the cooling effect of blood flow in a great artery.[15] Radiofrequency delivery at 60 W similarly increased the extent of acute microscopic injury to elastin and collagen fibers. More importantly, increasing radiofrequency power directly correlated with an increase in steam pop incidence and a shorter elapsed time-to-steam pop. These outcomes thus raise safety concerns about the use of high radiofrequency power, especially considering that the 60 W setting did not increase the likelihood of achieving radiofrequency lesions in the myocardium adjacent to the arterial wall.

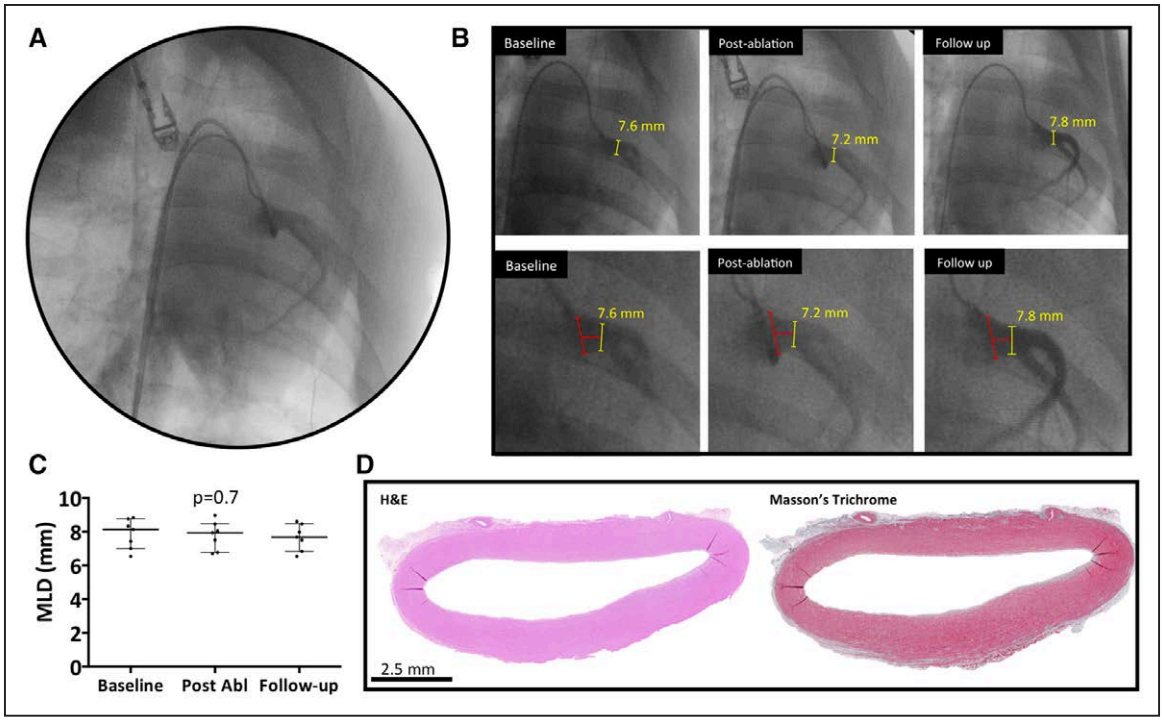

Figure 7. Coronary angiography and histology analysis of the left main coronary artery.
A, Sample angiogram of the left main coronary artery with the ablation catheter positioned in the left coronary sinus before radiofrequency delivery. **B**, Representative angiographic assessment of left main coronary artery diameter at baseline, post-ablation, and 1-month follow-up. Minimum lumen diameter (MLD, yellow lines) of the left main coronary artery was measured 5 mm from the ostium (distance from red to yellow lines) to avoid the variability associated with the funnel-like shape of the coronary ostium. **C**, MLD at baseline, post-ablation, and 1-month of follow-up in all group II animals. **D**, Representative hematoxylin and eosin (H&E) and Masson trichrome staining of the left main coronary artery ostium, showing the absence of coronary vessel injury 1 mo after radiofrequency delivery.

This finding suggests that, above a certain threshold, additional energy is absorbed by the arterial wall and surrounding intermediate tissue (eg, fat). Although their experimental design differs from ours, Calzolari et al[13] also reported an absence of significant correlation between power and lesion depth/width in an in vitro thigh preparation using 3 power settings at 20 W, 25 W, and 30 W. In another report, Yokoyama et al[12] showed that high power (50 W) and a low CF (2–10*g*) yielded smaller lesions than a 30 W setting and a CF range of 30*g* to 40*g*. In agreement with the Yokoyama et al[12] study, we also found that a median CF of ≈12*g* significantly decreased the likelihood of generating overt lesions in the myocardium adjacent to the arterial wall compared with a higher median CF value of ≈17*g*.

A key finding of our study is that the LSI, which integrates several factors involved in radiofrequency lesion formation,[13] predicted the presence of myocardial lesions adjacent to the arterial wall. A median LSI of 9.1 units was significantly associated with adjacent myocardial lesions compared with radiofrequency applications without adjacent lesions (median LSI=8.1 units). These data show that radiofrequency delivery to create myocardial lesions at the root of the aorta or pulmonary artery may require higher LSI values than those required for regular radiofrequency applications in direct contact with the myocardium.[13,14] For example, an LSI of just 8 units yielded large myocardial lesions in directly accessed heart preparations in vitro.[13] Moreover, recent data from in vivo experiments showed that and LSI of ≈5 units can achieve transmural lesions in the right atrium.[14] Our findings suggest that an LSI this low would not generate adjacent myocardial lesions during radiofrequency delivery from a great artery in vivo.

LSI values also showed a direct statistical trend toward an association with acute necrotic area in the myocardium adjacent to the arterial wall (*P*=0.1). However, high LSI values could increase the risk of steam pop and severe arterial wall damage if ablation parameters are not adjusted. Our experiments in the validation group documented that LSI values of ≈9 units, at 40 W radiofrequency, and CF values of ≈18*g* enabled the creation of effective and safe ablation lesions from the left coronary sinus. Moreover, titration of LSI by progressively increasing CF significantly increased the area of established adjacent myocardial lesions at 1-month follow-up as well as the extent of fibrotic remodeling, without causing vascular injury in the left main coronary artery. Importantly, these ablation parameters should be further adjusted in clinical practice by imposing a cutoff temperature of ≈38°C and avoiding excessive impedance falls (Tables 2 and 3).

Radiofrequency energy delivered at the aortic root has the potential to compromise long-term arterial wall integrity. However, wall stress testing after acute

increases in ascending aorta pressure did not detect any acute aortic rupture or dissection after 3 months of follow-up. Long-term integrity of the arterial wall after radiofrequency delivery was further supported by multiphoton microscopy analysis, which revealed recovery of both collagen and elastin fibers at the end of the follow-up period. To our knowledge, our study is the first to address this issue and provide evidence of artery recovery after radiofrequency lesions at the root of the aorta, regardless of whether the ablation target is a supravalvular myocardial sleeve in the arterial wall or adjacent myocardial tissue. It is important to note that none of the chronic lesions was associated with steam pop during radiofrequency delivery. The arterial wall integrity data, therefore, cannot be extrapolated to radiofrequency lesions occurring with steam pop, in which there was substantially greater wall damage (Figure 3) that may have given rise to safety issues during follow-up or wall stress testing.

Limitations

Although the in vivo pig model used here is of evident clinical relevance, ablation parameters may differ in a clinical setting. For example, the cutoff settings for temperature control during clinical applications are likely to differ, and this will alter power values. However, the experimental study design required uniform groups for comparison and precise evaluation of individual ablation parameters. Moreover, the LSI incorporates several factors involved in radiofrequency lesion formation, rather than power alone, which makes LSI a highly relevant parameter for monitoring radiofrequency delivery at the root of the aorta or pulmonary artery.

Clinical applications may also be affected by anatomic differences between pig and human hearts. For example, the fibrous barrier around the aortic valve is larger in humans,[22] and this could limit the size of ablation lesions. On the contrary, the coronary anatomy is similar in humans and pigs, which increases the clinical value of coronary assessment in pigs.[23]

Vascular steam pops during radiofrequency delivery were considered a potentially fatal threat (Figure 1 in the Data Supplement), although some lesions could have potentially recovered during the follow-up. However, long-term analyses of lesions with vascular steam pop during radiofrequency delivery were not performed in this study.

Conclusions

LSI titration using catheter-based CF technology and radiofrequency delivery at 40 W enables the creation of effective and safe ablation lesions from the root of the aorta or pulmonary artery. Further temperature control at ≈38°C with an impedance decrease of ≈16 ohms during radiofrequency delivery will prevent steam pops.

ARTICLE INFORMATION

Received May 9, 2018; accepted February 13, 2019.

The Data Supplement is available at https://www.ahajournals.org/doi/suppl/10.1161/CIRCEP.118.007080.

Correspondence

David Filgueiras-Rama, Centro Nacional de Investigaciones Cardiovasculares, Carlos III (CNIC), Myocardial Pathophysiology Area, Melchor Fernández Almagro, 3,28029 Madrid, Spain. Email david.filgueiras@cnic.es

Affiliations

Centro Nacional de Investigaciones Cardiovasculares, Carlos III (CNIC), Myocardial Pathophysiology Area (J.M.A.-A., J.G.Q., S.L.-C., J.J., D.F.-R.). Cardiovascular Institute, Department of Cardiology, Instituto de Investigación Sanitaria del Hospital Clínico San Carlos (IdISSC) (J.G.Q., J.J.G.-F., P.S., V.C.-G., L.B.-B., N.P.-C., J.P.-V.). CIBER de Enfermedades Cardiovasculares (J.G.Q., J.J.G.-F., V.C.-G., J.M., N.P.-C., J.J., J.P.-V., D.F.-R.). Fundación Interhospitalaria para la Investigación Cardiovascular (FIC) (M.J.G.-T., J.P.-V.). Experimental Medicine and Surgery Unit, Instituto de Investigación Sanitaria del Hospital Clínico San Carlos (IdISSC) (C.R.-B., P.G.). Hospital Universitario Ramón y Cajal, Department of Cardiology, Madrid, Spain (J.M.). Center for Arrhythmia Research, Cardiovascular Research Center, Department of Internal Medicine, University of Michigan, Ann Arbor (J.J.).

Acknowledgments

We are grateful for technical support provided by the animal facility at the Experimental Medicine and Surgery Unit, Instituto de Investigación Sanitaria del Hospital Clínico San Carlos (IdISSC) and the CNIC Microscopy Unit.

Sources of Funding

This study was supported by the Fundación Interhospitalaria para la Investigación Cardiovascular (FIC) and the Heart Rhythm Section of the Spanish Society of Cardiology. The Centro Nacional de Investigaciones Cardiovasculares (CNIC) is supported by the Ministry of Science, Innovation and Universities and the Pro CNIC Foundation. The CNIC is a Severo Ochoa Center of Excellence (SEV-2015-0505). This study was supported by grants from Fondo Europeo de Desarrollo Regional (CB16/11/00458) and the Spanish Ministry of Science, Innovation and Universities (SAF2016-80324-R).

Disclosures

None.

REFERENCES

1. Ganesan AN, Shipp NJ, Brooks AG, Kuklik P, Lau DH, Lim HS, Sullivan T, Roberts-Thomson KC, Sanders P. Long-term outcomes of catheter ablation of atrial fibrillation: a systematic review and meta-analysis. *J Am Heart Assoc*. 2013;2:e004549. doi: 10.1161/JAHA.112.004549
2. Keegan R, Aguinaga L, Fenelon G, Uribe W, Rodriguez Diez G, Scanavacca M, Patete M, Carhuaz RZ, Labadet C, De Zuloaga C, Pozzer D, Scazzuso F; SOLAECE registry investigators. The first Latin American Catheter Ablation Registry. *Europace*. 2015;17:794–800. doi: 10.1093/europace/euu322
3. Fontenla A, Garcia-Fernandez J, Ibanez JL, Spanish Catheter Ablation Registry collaborators. Spanish Catheter Ablation Registry. 16th official report of the Spanish Society of Cardiology Working Group on electrophysiology and arrhythmias (2016). *Rev Esp Cardiol (Engl Ed)*. 2017;70:971–982. doi: 10.1016/j.rec.2017.07.012
4. Yamada T, McElderry HT, Doppalapudi H, Murakami Y, Yoshida Y, Yoshida N, Okada T, Tsuboi N, Inden Y, Murohara T, Epstein AE, Plumb VJ, Singh SP, Kay GN. Idiopathic ventricular arrhythmias originating from the aortic root prevalence, electrocardiographic and electrophysiologic characteristics, and results of radiofrequency catheter ablation. *J Am Coll Cardiol*. 2008;52:139–147. doi: 10.1016/j.jacc.2008.03.040

5. Kanagaratnam L, Tomassoni G, Schweikert R, Pavia S, Bash D, Beheiry S, Neibauer M, Saliba W, Chung M, Tchou P, Natale A. Ventricular tachycardias arising from the aortic sinus of valsalva: an under-recognized variant of left outflow tract ventricular tachycardia. *J Am Coll Cardiol*. 2001;37:1408–1414.
6. Tada H, Naito S, Taniguchi K, Nogami A. Concealed left anterior accessory pathways: two approaches for successful ablation. *J Cardiovasc Electrophysiol*. 2003;14:204–208.
7. Beukema RJ, Smit JJ, Adiyaman A, Van Casteren L, Delnoy PP, Ramdat Misier AR, Elvan A. Ablation of focal atrial tachycardia from the noncoronary aortic cusp: case series and review of the literature. *Europace*. 2015;17:953–961. doi: 10.1093/europace/euu227
8. Suleiman M, Powell BD, Munger TM, Asirvatham SJ. Successful cryoablation in the noncoronary aortic cusp for a left anteroseptal accessory pathway. *J Interv Card Electrophysiol*. 2008;23:205–211. doi: 10.1007/s10840-008-9294-2
9. d'Avila A, Thiagalingam A, Holmvang G, Houghtaling C, Ruskin JN, Reddy VY. What is the most appropriate energy source for aortic cusp ablation? A comparison of standard RF, cooled-tip RF and cryothermal ablation. *J Interv Card Electrophysiol*. 2006;16:31–38. doi: 10.1007/s10840-006-9006-8
10. Pons M, Beck L, Leclercq F, Ferriere M, Albat B, Davy JM. Chronic left main coronary artery occlusion: a complication of radiofrequency ablation of idiopathic left ventricular tachycardia. *Pacing Clin Electrophysiol*. 1997;20:1874–1876.
11. Aliot EM, Stevenson WG, Almendral-Garrote JM, Bogun F, Calkins CH, Delacretaz E, Della Bella P, Hindricks G, Jaïs P, Josephson ME, Kautzner J, Kay GN, Kuck KH, Lerman BB, Marchlinski F, Reddy V, Schalij MJ, Schilling R, Soejima K, Wilber D; European Heart Rhythm Association (EHRA); Registered Branch of the European Society of Cardiology (ESC); Heart Rhythm Society (HRS); American College of Cardiology (ACC); American Heart Association (AHA). EHRA/HRS expert consensus on catheter ablation of ventricular arrhythmias: developed in a partnership with the European Heart Rhythm Association (EHRA), a registered branch of the European Society of Cardiology (ESC), and the Heart Rhythm Society (HRS); in collaboration with the American College of Cardiology (ACC) and the American Heart Association (AHA). *Heart Rhythm*. 2009;6:886–933. doi: 10.1016/j.hrthm.2009.04.030
12. Yokoyama K, Nakagawa H, Shah DC, Lambert H, Leo G, Aeby N, Ikeda A, Pitha JV, Sharma T, Lazzara R, Jackman WM. Novel contact force sensor incorporated in irrigated radiofrequency ablation catheter predicts lesion size and incidence of steam pop and thrombus. *Circ Arrhythm Electrophysiol*. 2008;1:354–362. doi: 10.1161/CIRCEP.108.803650
13. Calzolari V, De Mattia L, Indiani S, Crosato M, Furlanetto A, Licciardello C, Squasi PAM, Olivari Z. *In vitro* validation of the lesion size index to predict lesion width and depth after irrigated radiofrequency ablation in a porcine model. *JACC Clin Electrophysiol*. 2017;3:1126–1135. doi: 10.1016/j.jacep.2017.08.016
14. Whitaker J, Fish J, Harrison J, Chubb H, Williams SE, Fastl T, Corrado C, Van Zaen J, Gibbs J, O'Neill L, Mukherjee R, Rittey D, Thorsten J, Donskoy E, Sohal M, Rajani R, Niederer S, Wright M, O'Neill MD. Lesion index-guided ablation facilitates continuous, transmural, and durable lesions in a porcine recovery model. *Circ Arrhythm Electrophysiol*. 2018;11:e005892. doi: 10.1161/CIRCEP.117.005892
15. Moreno J, Quintanilla JG, Molina-Morúa R, García-Torrent MJ, Angulo-Hernández MJ, Curiel-Llamazares C, Ramiro-Bargueño J, González P, Caamaño AJ, Pérez-Castellano N, Rojo-Álvarez JL, Macaya C, Pérez-Villacastín J. Morphological and thermodynamic comparison of the lesions created by 4 open-irrigated catheters in 2 experimental models. *J Cardiovasc Electrophysiol*. 2014;25:1391–1399. doi: 10.1111/jce.12528
16. Başkaya MK, Doğan A, Temiz C, Dempsey RJ. Application of 2,3,5-triphenyltetrazolium chloride staining to evaluate injury volume after controlled cortical impact brain injury: role of brain edema in evolution of injury volume. *J Neurotrauma*. 2000;17:93–99. doi: 10.1089/neu.2000.17.93
17. Schneider CA, Rasband WS, Eliceiri KW. NIH Image to ImageJ: 25 years of image analysis. *Nat Methods*. 2012;9:671–675.
18. Hou L, Liu K, Li Y, Ma S, Ji X, Liu L. Necrotic pyknosis is a morphologically and biochemically distinct event from apoptotic pyknosis. *J Cell Sci*. 2016;129:3084–3090. doi: 10.1242/jcs.184374
19. Leshem E, Tschabrunn CM, Contreras-Valdes FM, Zilberman I, Anter E. Evaluation of ablation catheter technology: Comparison between thigh preparation model and an *in vivo* beating heart. *Heart Rhythm*. 2017;14:1234–1240. doi: 10.1016/j.hrthm.2017.04.035
20. Guerra JM, Jorge E, Raga S, Gálvez-Montón C, Alonso-Martín C, Rodríguez-Font E, Cinca J, Viñolas X. Effects of open-irrigated radiofrequency ablation catheter design on lesion formation and complications: *in vitro* comparison of 6 different devices. *J Cardiovasc Electrophysiol*. 2013;24:1157–1162. doi: 10.1111/jce.12175
21. Nakagawa H, Yamanashi WS, Pitha JV, Arruda M, Wang X, Ohtomo K, Beckman KJ, McClelland JH, Lazzara R, Jackman WM. Comparison of *in vivo* tissue temperature profile and lesion geometry for radiofrequency ablation with a saline-irrigated electrode versus temperature control in a canine thigh muscle preparation. *Circulation*. 1995;91:2264–2273.
22. Crick SJ, Sheppard MN, Ho SY, Gebstein L, Anderson RH. Anatomy of the pig heart: comparisons with normal human cardiac structure. *J Anat*. 1998;193(pt 1):105–119.
23. Weaver ME, Pantely GA, Bristow JD, Ladley HD. A quantitative study of the anatomy and distribution of coronary arteries in swine in comparison with other animals and man. *Cardiovasc Res*. 1986;20:907–917.